PROCEEDINGS OF SCIENCE

Proton structure in the hyperfine splitting of muonic hydrogen

Franziska Hagelstein[*†] **and Vladimir Pascalutsa**
Institut für Kernphysik, Johannes Gutenberg Universität, Mainz, Germany
E-mail: hagelste@uni-mainz.de

We present the leading-order prediction of baryon chiral perturbation theory for the proton polarizability contribution to the $2S$ hyperfine splitting in muonic hydrogen, and compare to the results of dispersive calculations.

The 8th International Workshop on Chiral Dynamics
29 June 2015 - 03 July 2015
Pisa, Italy

[*]Speaker.

[†]This work was supported by the Deutsche Forschungsgemeinschaft (DFG) through the Collaborative Research Center SFB 1044 [The Low-Energy Frontier of the Standard Model], and the Graduate School DFG/GRK 1581 [Symmetry Breaking in Fundamental Interactions].

PoS(CD15)077

1. Introduction

The apparent discrepancy between extractions of the proton radius from experiments performed with electronic [1, 2, 3] vs. muonic probes [4, 5] – *aka* the proton-size puzzle – calls for a precise theoretical understanding of the hydrogen spectrum.

The extraction of the proton charge radius R_E and the Zemach radius R_Z from muonic hydrogen (μH) spectroscopy relies on a comparison between measured transition frequencies in the hydrogen atom [4] and theoretical predictions for the hydrogen spectrum. The description of the classic $2P-2S$ Lamb shift and the $2S$ hyperfine splitting (HFS) in μH is given by (in units of meV) [5]:

$$\Delta E^{\rm th}_{\rm LS} = 206.0336(15) - 5.2275(10)\,(R_E/{\rm fm})^2 + \Delta E^{\rm TPE}_{\rm LS}, \quad \text{with } \Delta E^{\rm TPE}_{\rm LS} = 0.0332(20), \tag{1.1a}$$

$$\Delta E^{\rm th}_{2S\,\rm HFS} = 22.9763(15) - 0.1621(10)\,(R_Z/{\rm fm}) + \Delta E^{\rm pol}_{2S\,\rm HFS}, \quad \text{with } \Delta E^{\rm pol}_{2S\,\rm HFS} = 0.0080(26), \tag{1.1b}$$

where the first number includes the QED effects, as well as their interference with the leading order (LO) finite-size effect, i.e., R_E; $\Delta E^{\rm TPE}_{\rm LS}$ stands for the proton structure effects beyond the LO, precisely, the Friar radius, recoil finite-size effects, and the polarizability effect; $\Delta E^{\rm pol}_{2S\,\rm HFS}$ is the polarizability effect in the HFS.

In the future, a measurement of the μH ground-state HFS (see, e.g., Sect. 6 of Ref. [6]) could enhance our understanding of the proton structure. Such experiment requires a precise theoretical prediction for the $1S$ HFS, because the transition is very narrow. At present, the biggest uncertainty lies in the two-photon exchange polarizability contribution to the HFS. We investigate both the finite-size and the polarizability effects on the HFS.

2. Finite-size effects by dispersive technique

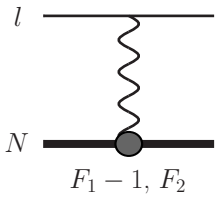

Figure 1: One-photon exchange with form factor dependent electromagnetic vertex. Here, l represents the lepton and N the nucleon.

In a recent paper [7], we study the applicability of the expansion of finite-size corrections to the Lamb shift in moments of the charge distribution. We now present an extension of this work to the HFS.

Figure 1 shows the one-photon exchange in an atomic bound state. It can be calculated using the electromagnetic vertex:

$$\Gamma^\mu = Z\gamma^\mu F_1(Q^2) - \frac{1}{2M}\gamma^{\mu\nu}q_\nu F_2(Q^2), \quad (Z=1 \text{ for the proton}) \tag{2.1}$$

with the proton structure information embedded in the Dirac and Pauli form factors, F_1 and F_2, and the photon propagator in massive Coulomb gauge:

$$\Delta_{\mu\nu}(q,t) = -\frac{1}{q^2}\left[g_{\mu\nu} - \frac{1}{\mathbf{q}^2+t}\left(q_\mu q_\nu - \chi_\mu q_\nu - \chi_\nu q_\mu\right)\right], \quad \text{with } \chi = (0,\mathbf{q}). \tag{2.2}$$

Assuming that the nucleon form factors fulfill once-subtracted dispersion relations,

$$\begin{pmatrix} F_1(Q^2) \\ F_2(Q^2) \end{pmatrix} = \begin{pmatrix} 1 \\ \varkappa \end{pmatrix} + \frac{q^2}{\pi}\int_{t_0}^{\infty} \frac{\mathrm{d}t}{t(t-q^2)}\,\mathrm{Im}\begin{pmatrix} F_1(t) \\ F_2(t) \end{pmatrix}, \tag{2.3}$$

with t_0 being the lowest particle-production threshold and $q^2 = -Q^2$ the virtuality of the exchanged photon, we can deduce the following one-photon exchange (coordinate space) Breit potential:

$$V_{\text{F.S.}}(\mathbf{r},t) = \frac{Z\alpha}{\pi r}\int_{t_0}^{\infty}\frac{\mathrm{d}t}{t}e^{-r\sqrt{t}}\,\mathrm{Im}\,G_E(t), \tag{2.4a}$$

$$V^{l=0}_{\text{HFS,a}}(\mathbf{r},t) = \frac{Z\alpha}{3}\frac{1+\varkappa}{mM}\left[f(f+1)-\frac{3}{2}\right]4\pi\,\delta(\mathbf{r}), \tag{2.4b}$$

$$V^{l=0}_{\text{HFS,b}}(\mathbf{r},t) = -\frac{4Z\alpha}{3}\frac{1+\varkappa}{mM}\left[f(f+1)-\frac{3}{2}\right]\left(\delta(\mathbf{r})\int_{t_0}^{\infty}\frac{\mathrm{d}t}{t}\frac{\mathrm{Im}\,G_M(t)}{1+\varkappa} - \pi\rho_M(r)\right), \tag{2.4c}$$

$$\vdots$$

where we substituted the electric and magnetic Sachs form factors:

$$G_E(Q^2) = F_1(Q^2) - \tau F_2(Q^2), \quad G_M(Q^2) = F_1(Q^2) + F_2(Q^2), \tag{2.5}$$

with $\tau = Q^2/4M^2$. Hereinafter, m refers to the muon mass, M is the proton mass, $\varkappa$ is the anomalous magnetic moment of the proton, l is the orbital angular momentum ($l=0$ for S-waves), f is the atom's total angular momentum and ρ_M is the magnetization density:

$$\rho_M(r) = \int\frac{\mathrm{d}\mathbf{Q}}{(2\pi)^3}\frac{G_M(Q^2)}{1+\varkappa}e^{i\mathbf{Q}\cdot\mathbf{r}} = \frac{1}{(2\pi)^2 r}\int_{t_0}^{\infty}\mathrm{d}t\,\frac{\mathrm{Im}\,G_M(t)}{1+\varkappa}\,e^{-r\sqrt{t}}. \tag{2.6}$$

At 1$^{\text{st}}$-order in time-independent perturbation theory (PT), the Lamb shift due to the Yukawa-type correction in Eq. (2.4a) is given by:

$$E_{\text{LS}}^{\text{FSE}\,(1)} = -\frac{Z\alpha}{2\pi a^3}\int_{t_0}^{\infty}\mathrm{d}t\,\frac{\mathrm{Im}\,G_E(t)}{(\sqrt{t}+Z\alpha m_r)^4}, \tag{2.7a}$$

$$= -\frac{Z\alpha}{12a^3}\sum_{k=0}^{\infty}\frac{(-Z\alpha m_r)^k}{k!}\langle r^{k+2}\rangle_E, \tag{2.7b}$$

or equivalently,

$$E_{\text{LS}}^{\text{FSE}\,(1)} = \int_0^{\infty}\mathrm{d}Q\,w_E(Q)\,G_E(Q^2), \quad \text{with } w_E(Q) = -\frac{4Z\alpha}{\pi a^4}\frac{Q^2\left[(Z\alpha m_r)^2 - Q^2\right]}{\left[(Z\alpha m_r)^2+Q^2\right]^4}, \tag{2.8}$$

where m_r is the reduced mass of the muon-proton system and $a = (Z\alpha m_r)^{-1}$ is the Bohr radius. In deriving Eq. (2.7b), we have expanded in the moments of the charge distribution, using the following (Lorentz-invariant) definition:

$$\langle r^N\rangle_E = \frac{(N+1)!}{\pi}\int_{t_0}^{\infty}\mathrm{d}t\,\frac{\mathrm{Im}\,G_E(t)}{t^{N/2+1}}, \quad \text{where } R_E = \sqrt{\langle r^2\rangle_E}. \tag{2.9}$$

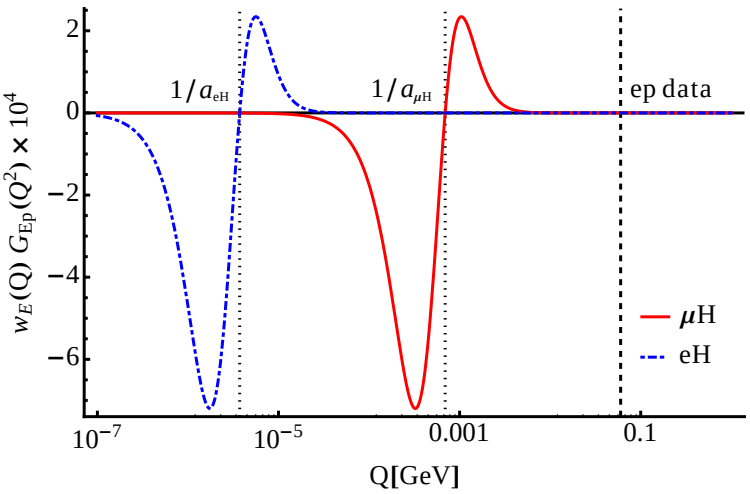

Figure 2: Integrand of the 1st-order PT contribution to the Lamb shift [cf. Eq. (2.8)] of eH (blue dash-dotted line) and of μH (red solid line) for the dipole FF, $G_{Ep} = (1+Q^2/0.71\,\mathrm{GeV}^2)^{-2}$. The dotted vertical lines indicate the inverse Bohr radii of the two hydrogens, while the vertical dashed line indicates the onset of the elastic electron-proton scattering data.

However, from the denominator of Eq. (2.7a) one can see that the convergence radius of the power-series expansion is limited by t_0, i.e., the proximity of the nearest particle-production threshold. The exact (non-expanded) finite-size effect on the Lamb shift, cf. Eq. (2.8), is the result of large cancelations around the Bohr radius scale, see Fig. 2. We conclude that soft contributions to the proton or lepton electric form factor, at energies comparable to the inverse Bohr radius, can break down the expansion, and accordingly, limit the usual accounting of finite-size effects which is presented in Eq. (1.1a). Therefore, one has to know all the soft contributions to the proton electric form factor to high accuracy for an accurate extraction of R_E from the Lamb shift in μH.

Analogously, we establish the exact finite-size effect on the HFS, starting from the spin-dependent part of the Breit potential, cf. Eqs. (2.4b) and (2.4c). Treating the potential (2.4b) at 1st-order in PT, we reproduce the LO HFS, which is given by the well-known Fermi energy:

$$E_F(nS) = \frac{8Z\alpha}{3a^3}\frac{1+\varkappa}{mM}\frac{1}{n^3} \overset{n=2}{=} 22.8054\,\mathrm{meV}. \tag{2.10}$$

Applying 1st-order PT to Eq. (2.4c) leads to:

$$E_{2S\,\mathrm{HFS}}^{\mathrm{HFS,b\,(1)}} = -\frac{E_F(2S)}{\pi}\int_{t_0}^{\infty}\mathrm{d}t\left(\frac{1}{t}-\frac{2t+(Z\alpha m_r)^2}{2[\sqrt{t}+Z\alpha m_r]^4}\right)\frac{\mathrm{Im}\,G_M(t)}{1+\varkappa}, \tag{2.11a}$$

$$= -E_F(2S)\left\{1-\frac{4}{\pi a}\int_0^{\infty}\mathrm{d}Q\frac{Q^2\left[(Z\alpha m_r)^2-Q^2\right]\left[(Z\alpha m_r)^2-2Q^2\right]}{\left[(Z\alpha m_r)^2+Q^2\right]^4}\frac{G_M(Q^2)}{1+\varkappa}\right\}, \tag{2.11b}$$

$$= -E_F(2S)\left\{1-8\pi a^3\int_0^{\infty}\mathrm{d}r\,r^2\left[R_{20}(r)\right]^2\rho_M(r)\right\}, \tag{2.11c}$$

with the radial Coulomb wave function $R_{20}(r) = {}^1\!/\!_{\sqrt{2}a^{3/2}}\,(1-{}^r\!/\!_{2a})\,e^{-r/2a}$. Reading off Eqs. (2.11c) and (2.10), the combined 1st-order result is entirely expressed as an integral over the magnetization density. The corresponding integrand is plotted in Fig. 3 for the dipole FF. Again, one observes an

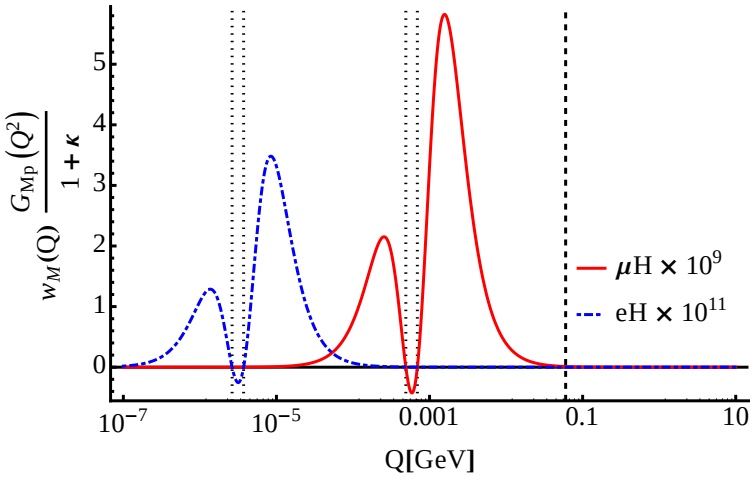

Figure 3: Integrand of the 1st-order PT contribution to the $2S$ HFS [cf. Eq. (2.10) and Eq. (2.11b), here $w_M(Q) = \frac{4E_F(2S)}{\pi a}\frac{Q^2\left[(Z\alpha m_r)^2-Q^2\right]\left[(Z\alpha m_r)^2-2Q^2\right]}{\left[(Z\alpha m_r)^2+Q^2\right]^4}$] of eH (blue dash-dotted line) and of μH (red solid line) for the dipole FF, $G_{Mp} = (1+\varkappa)(1+Q^2/0.71\,\mathrm{GeV}^2)^{-2}$. The dotted vertical lines indicate scales related to the inverse Bohr radii of the two hydrogens, particularly $1/a$ and $1/\sqrt{2}a$, while the vertical dashed line indicates the onset of the elastic electron-proton scattering data.

enhancement of the integrand for small values of Q, which emphasizes the necessity for an exact evaluation of soft contributions to the form factors.

3. Polarizability contribution to the HFS

In this section, we give a baryon chiral perturbation theory (BChPT) prediction for the pion contribution to the polarizability effect on the $2S$ HFS in μH, cf. $\Delta E^{\mathrm{pol}}_{2S\,\mathrm{HFS}}$ from Eq. (1.1b).

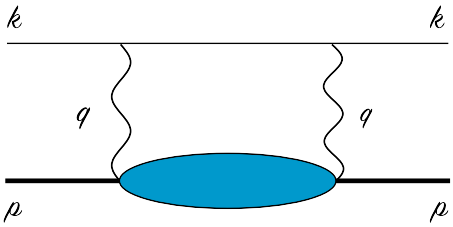

Figure 4: TPE diagram in forward kinematics: the horizontal lines correspond to the lepton and the proton (bold), where the "blob" represents forward doubly-virtual Compton scattering.

Figure 4 shows the (forward) two-photon exchange (TPE) in an atomic bound state, which contributes to the HFS and the Lamb shift at next-to-leading order. Fading out the lepton line in Fig. 4, one obtains the doubly-virtual Compton scattering process (VVCS). For the required accuracy, $O(\alpha^5)$, it is sufficient to study only the forward limit, i.e., $q' = q$ (hence, $p' = p$, $t = 0$). The tensor decomposition of the forward VVCS amplitude then splits into symmetric and

antisymmetric parts:

$$T^{\mu\nu}(q,p) = T_S^{\mu\nu} + T_A^{\mu\nu}, \tag{3.1a}$$

$$T_S^{\mu\nu}(q,p) = -g^{\mu\nu}T_1(\nu,Q^2) + \frac{p^\mu p^\nu}{M^2}T_2(\nu,Q^2), \tag{3.1b}$$

$$T_A^{\mu\nu}(q,p) = \frac{1}{M}\gamma^{\mu\nu\alpha}q_\alpha S_1(\nu,Q^2) - \frac{Q^2}{M^2}\gamma^{\mu\nu}S_2(\nu,Q^2), \tag{3.1c}$$

with $T_{1,2}$ the spin-independent and $S_{1,2}$ the spin-dependent invariant amplitudes, functions of the photon (lab-frame) energy ν and the photon virtuality $Q^2 = -q^2$. The spin-dependent part of the Compton process contributes to the HFS, whereas the spin-independent part contributes to the Lamb shift. The TPE correction to the HFS of the n-th S-level is given by [8]:

$$E_{nS\mathrm{HFS}}^{\mathrm{pol}} = \frac{mE_F(nS)}{2(1+\varkappa)\pi^4}\frac{1}{i}\int_0^\infty \mathrm{d}\nu \int \mathrm{d}\mathbf{q}\,\frac{1}{Q^4-4m^2\nu^2}\left\{\frac{(2Q^2-\nu^2)}{Q^2}S_1(\nu,Q^2)+3\frac{\nu}{M}S_2(\nu,Q^2)\right\}, \tag{3.2}$$

where E_F is the hydrogen Fermi energy, i.e., the LO HFS. The TPE can be divided into an "elastic" and an "inelastic" part. As mentioned previously, we are only interested in the "polarizability", or "inelastic", contribution given by the non-Born part of the Compton amplitudes.

All invariant amplitudes are related to photoabsorption cross sections by sum rules, however, the amplitude T_1 requires a once-subtracted dispersion relation. Therefore, in contrast to the HFS, the polarizability contribution to the Lamb shift is not determined by empirical information (on nucleon form factors, and structure functions or photoabsorption cross sections) alone and requires a rigorous theoretical input. Such an input has been provided by the recent BChPT calculation of Alarcón et al. [9]. We extend this calculation to the HFS, where the BChPT framework is put to the test by the available dispersive calculations [8, 10, 11, 12, 13]. Moreover, we address the contributions to the HFS by pion exchange, which are off-forward and not covered by Eq. (3.2).

3.1 BChPT at leading order

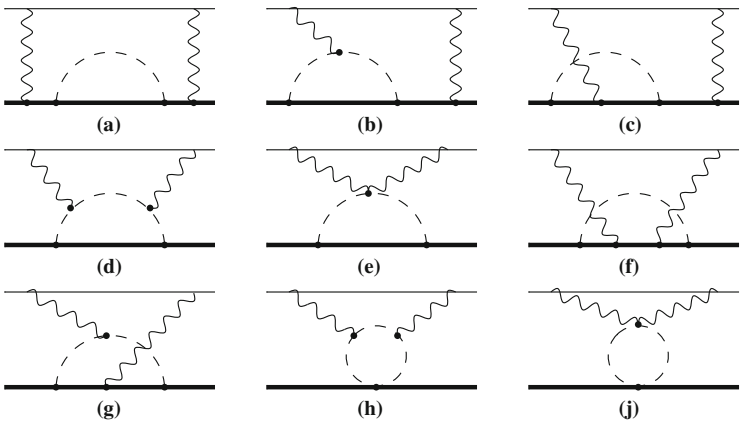

Figure 5: The TPE diagrams of elastic lepton-nucleon scattering to $O(p^3)$ in BChPT. Diagrams obtained from these by crossing and time-reversal symmetry are not drawn. Reproduced from Ref. [9].

The pion-nucleon loop contribution to the HFS, shown in Fig. 5, is evaluated based on Eq. (3.2). Substituting the Compton amplitudes from Ref. [9], we obtain the $2S$ HFS in μH:

$$E_{2S\,\mathrm{HFS}}^{(\pi N\,\mathrm{loops})} = 0.85 \pm 0.42\,\mu\mathrm{eV}. \tag{3.3}$$

This is the pure "polarizability" contribution, i.e., corrections due to elastic form factors have been subtracted. Figure 6 shows the dependence of the pion-nucleon loop polarizability contribution (green line) on a momentum-cutoff. We estimate the error with 50 %, what is illustrated by the green band.

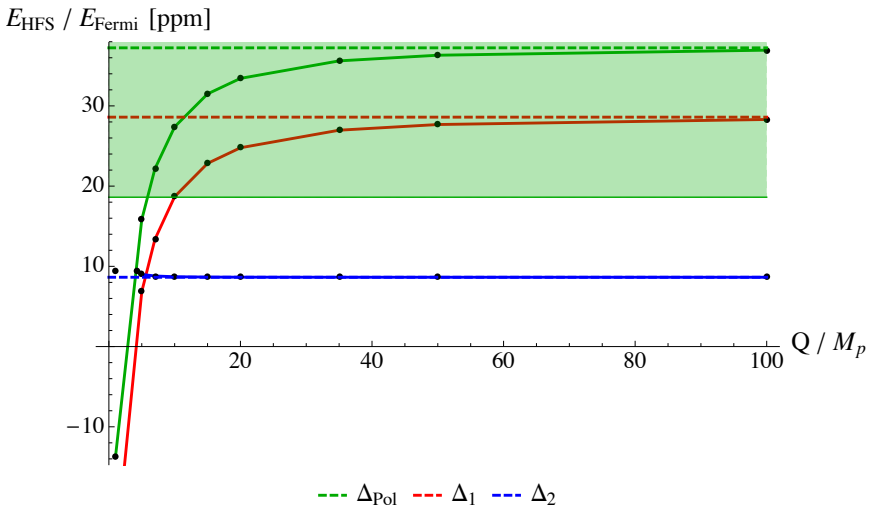

Figure 6: Cutoff-dependence of the pion-nucleon loop contribution. Here, Δ_1 and Δ_2 represent the contributions due to S_1 and S_2, respectively. Δ_{pol} is the sum of Δ_1 and Δ_2. The dashed lines are without momentum-cutoff.

3.2 Remarks on π^0 exchange

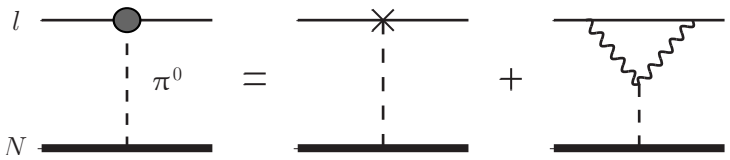

Figure 7: π^0 exchange in an atomic bound state. Here, l represents the lepton and N the nucleon.

Figure 7 shows the neutral-pion exchange in an atomic bound state. This process is vanishing in the forward limit, but gives a $O(\alpha^6)$ contribution for off-forward scattering. For the HFS contribution we obtain:

$$E_{nS\,\mathrm{HFS}}^{(\pi^0)} = -E_F(nS)\frac{\alpha^2}{2\pi(1+\varkappa_p)}\frac{m_r}{m_\pi}g_{\pi NN}\left[g_{\pi\ell\ell}+\frac{m}{2\pi^2 f_\pi}I(\kappa)\right], \tag{3.4}$$

where $\kappa = m_\pi/2m$, and

$$I(\kappa) \equiv 2\int_0^\infty \frac{\mathrm{d}\zeta}{1+\zeta/\kappa}\frac{\arccos\zeta}{\sqrt{1-\zeta^2}}. \tag{3.5}$$

Note that the first term is due to the diagram with the pion directly coupling to the lepton and the second term is due to the diagram with two-photon coupling to the lepton. The $\pi\ell\ell$ coupling can be extract from the decay width of $\pi^0 \to e^+e^-$:

$$\Gamma(\pi^0 \to e^+e^-) = \frac{m_\pi}{8\pi}\sqrt{1-\frac{4m_e^2}{m_\pi^2}}\left|F(m_\pi^2,m_e^2,m_e^2)\right|^2, \tag{3.6}$$

with m_π and m_e being the mass of pion and electron, respectively. Since the $\pi\ell\ell$ coupling is given by:

$$g_{\pi\ell\ell} = F(0,m_\ell^2,m_\ell^2)/\alpha^2, \tag{3.7}$$

an interpolation between the pion momenta $q^2 = 0$ and m_π^2 is required. To leading order in α, the form factor might be written as [14]:

$$F(q^2) \equiv F(q^2,m_\ell^2,m_\ell^2) = F(0) + \frac{q^2}{\pi}\int_0^\infty \frac{\mathrm{d}s}{s}\frac{\mathrm{Im}\,F(s)}{s-q^2}, \tag{3.8a}$$

$$\mathrm{Im}\,F(s) = -\frac{\alpha^2 m_\ell}{2\pi f_\pi}\frac{\mathrm{arccosh}(\sqrt{s}/2m_\ell)}{\sqrt{1-4m_\ell^2/s}}, \tag{3.8b}$$

$$F(0) = \frac{\alpha^2 m_\ell}{2\pi^2 f_\pi}\left(\mathscr{A}(\Lambda) + 3\ln\frac{m_\ell}{\Lambda}\right), \tag{3.8c}$$

where f_π is the pion-decay constant, Λ is the renormalization scale, and $\mathscr{A}$ is a universal pion-lepton low-energy constant, related to the physical constant in an obvious way:

$$g_{\pi\ell\ell} = \frac{m_\ell}{2\pi^2 f_\pi}\mathscr{A}(m_\ell). \tag{3.9}$$

From the experimental $\pi^0 \to e^+e^-$ decay width one finds: $\mathscr{A}(m_e) = -20(1)$. The value of the muon coupling we then find as: $\mathscr{A}(m) = \mathscr{A}(m_e) + 3\ln(m/m_e) = -4(1)$, with the muon mass m. The πNN coupling can be approximated by the Goldberger-Treiman relation [15]:

$$g_{\pi NN} = M g_A/f_\pi, \tag{3.10}$$

with the axial coupling $g_A \approx 1.27$ and $f_\pi \approx 92.4\,\mathrm{MeV}$. Finally, the HFS of the $2S$ level in μH amounts to:

$$E_{2S\,\mathrm{HFS}}^{(\pi^0)} = 0.02 \pm 0.04\,\mu\mathrm{eV}. \tag{3.11}$$

Recently, the effect of the pion exchange has also been estimated by Huong et al. [16] and Zhou et al. [17]. The result of Ref. [16], $E_{2S\,\mathrm{HFS}}^{(\pi^0)} = -(0.09 \pm 0.06)\,\mu\mathrm{eV}$, is comparable to our result. Whereas the latter find the diagram with two-photon coupling (cf. Fig. 7) to dominate, and arrive at a two orders of magnitude larger contribution: $E_{2S\,\mathrm{HFS}}^{(\pi^0)} = 2.8\,\mu\mathrm{eV}$ [17]. However, they simply evaluated the ultraviolet-divergent loop in Fig. 7 by imposing an arbitrary cutoff and did not check whether their result is consistent with the $\pi^0 \to e^+e^-$ decay width.

4. Discussion and conclusion

Combining the individual pion contributions, Eqs. (3.11) and (3.3), we arrive at:

$$E_{2S\,\mathrm{HFS}}^{(\pi^0\,\&\,\pi N\,\mathrm{loops})} = 0.87 \pm 0.42\,\mu\mathrm{eV}. \tag{4.1}$$

Figure 8 shows a comparison between our BChPT prediction for the polarizability contribution to the $2S$ HFS in μH and other predictions based on dispersive approaches [8, 10, 11, 12, 13]. Apparently, the two methods do not give consistent results; our prediction is considerably smaller.

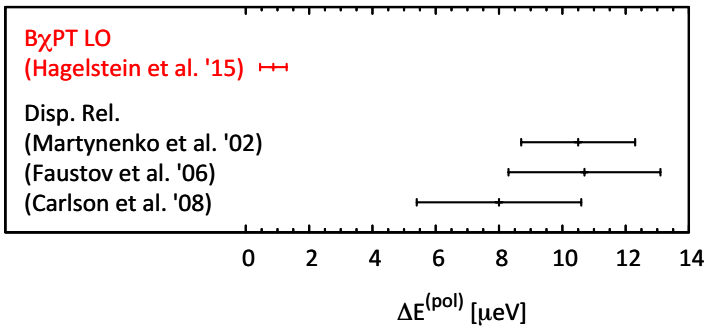

Figure 8: Comparison of predictions for the $2S$ HFS in μH. The dispersive calculations are from Refs. [8, 10, 11, 12, 13].

However, one should mention that the LO BChPT prediction for the Lamb shift [9] is in good agreement with dispersive calculations, e.g., [18, 19], despite the fact that the Lamb shift calculations involve a so-called "subtraction term", corresponding to the subtraction in the T_1 dispersion relation, which can only be modeled within the dispersive approaches.

For future work, one has to investigate if there are higher-order corrections contributing non-negligibly to the BChPT prediction, e.g., through the Δ-excitation.

Further details of our calculation, as well as a more elaborate discussion, can be found in Ref. [20].

References

[1] P. J. Mohr, B. N. Taylor and D. B. Newell, *CODATA recommended values of the fundamental physical constants: 2010*, Rev. Mod. Phys. **84** (2012) 1527 [atom-ph/1203.5425].

[2] J. C. Bernauer, et al. [A1 Collaboration], *High-precision determination of the electric and magnetic form factors of the proton*, Phys. Rev. Lett. **105** (2010) 242001 [nucl-ex/1007.5076].

[3] X. Zhan, K. Allada, D. S. Armstrong, J. Arrington, W. Bertozzi, W. Boeglin, J.-P. Chen, K. Chirapatpimol, et al., *High precision measurement of the proton elastic form factor ratio* $\mu_p G_E/G_M$ *at low* Q^2, Phys. Lett. B **705** (2011) 59 [nucl-ex/1102.0318].

[4] A. Antognini, F. Nez, K. Schuhmann, F. D. Amaro, F. Biraben, J. M. R. Cardoso, D. S. Covita, A. Dax, et al., *Proton structure from the measurement of* $2S-2P$ *transition frequencies of muonic hydrogen*, Science **339** (2013) 417.

[5] A. Antognini, F. Kottmann, F. Biraben, P. Indelicato, F. Nez and R. Pohl, *Theory of the 2S-2P Lamb shift and 2S hyperfine splitting in muonic hydrogen*, Annals Phys. **331** (2013) 127 [atom-ph/1208.2637].

[6] A. Antognini, *Muonic atoms and the nuclear structure*, in: Proceedings, 22nd International Conference on Laser Spectroscopy (ICOLS 2015), Singapore, June 28 – July 3 [atom-ph/1512.01765].

[7] F. Hagelstein and V. Pascalutsa, *Breakdown of the expansion of finite-size corrections to the hydrogen Lamb shift in moments of charge distribution*, Phys. Rev. A **91** (2015) 040502 [hep-ph/1502.03721].

[8] C. E. Carlson, V. Nazaryan and K. Griffioen, *Proton structure corrections to hyperfine splitting in muonic hydrogen*, Phys. Rev. A **83** (2011) 042509 [atom-ph/1101.3239].

[9] J. M. Alarcón, V. Lensky and V. Pascalutsa, *Chiral perturbation theory of muonic hydrogen Lamb shift: polarizability contribution*, Eur. Phys. J. C **74** (2014) 2852 [hep-ph/1312.1219].

[10] C. E. Carlson, V. Nazaryan and K. Griffioen, *Proton structure corrections to electronic and muonic hydrogen hyperfine splitting*, Phys. Rev. A **78** (2008) 022517 [atom-ph/0805.2603].

[11] R. N. Faustov, I. V. Gorbacheva and A. P. Martynenko, *Proton polarizability effect in the hyperfine splitting of the hydrogen atom*, Proc. SPIE Int. Soc. Opt. Eng. **6165** (2006) 0M [hep-ph/0610332].

[12] R. N. Faustov, E. V. Cherednikova and A. P. Martynenko, *Proton polarizability contribution to the hyperfine splitting in muonic hydrogen*, Nucl. Phys. A **703** (2002) 365-377 [hep-ph/0108044].

[13] A. P. Martynenko, *2S hyperfine splitting of muonic hydrogen*, Phys. Rev. A **71** (2005) 022506 [hep-ph/0409107].

[14] S. Drell, *Direct decay* $\pi^0 \to e^+ + e^-$, Il Nuovo Cimento **11** (1959) 693-697.

[15] M. L. Goldberger and S.B. Treiman, *Decay of the* π *meson*, Phys. Rev. **110** (1958) 1178-1184; M. L. Goldberger and S.B. Treiman, *Form-factors in* β *decay and* μ *capture*, Phys. Rev. **111** (1958) 354-361.

[16] N. T. Huong, E. Kou, B. Moussallam, *Single pion contribution to the hyperfine splitting in muonic hydrogen*, hep-ph/1511.06255 (2015).

[17] H.-Q. Zhou, H.-R. Pang, *One-pion-exchange effect in the energy spectrum of muonic hydrogen*, Phys. Rev. A **92** (2015) 032512.

[18] C. E. Carlson, M. Vanderhaeghen, *Higher order proton structure corrections to the Lamb shift in muonic hydrogen*, Phys. Rev. A **84** (2011) 020102 [hep-ph/1101.5965].

[19] M. C. Birse and J. A. McGovern, *Proton polarisability contribution to the Lamb shift in muonic hydrogen at fourth order in chiral perturbation theory*, Eur. Phys. J. A **48** (2012) 120 [hep-ph/1206.3030].

[20] F. Hagelstein, R. Miskimen and V. Pascalutsa, *Nucleon Polarizabilities: from Compton Scattering to Hydrogen Atom*, Prog. Part. Nucl. Phys. (2015), http://dx.doi.org/10.1016/j.ppnp.2015.12.001 [nucl-th/1512.03765].